Air-Filled Long Slot Leaky-Wave Antenna Based on Folded Half-Mode Waveguide Using Silicon Bulk Micromachining Technology for Millimeter-Wave Band

Le Chang, *Student Member, IEEE*, Zhijun Zhang, *Fellow, IEEE*, Yue Li, *Member, IEEE*, Shaodong Wang, and Zhenghe Feng, *Fellow, IEEE*

***Abstract*— An air-filled long slot leaky-wave antenna (LWA) based on folded half-mode waveguide (FHMW) fabricated using silicon substrate is proposed for millimeter-wave application. As is well known, the high-permittivity silicon dielectric is not suitable for antenna design. Thanks to the through-wafer dry etching and gold-plating processes deriving from the silicon bulk micromachining technology, three purely air-filled structures including the vertical part of the FHMW that also acts as the leaky-wave long slot in the top layer, horizontal part of the FHMW and matching section in the middle layer, and coupling slot in the bottom layer constitute the high-performance air-filled long slot LWA. To the best of the authors' knowledge, this is the first time that an FHMW is adopted for antenna design. Compared with the conventional half-mode waveguide, the profile is lowered, the required silicon layer number is fixed to three, and the design can be more flexible. Experiment of the fabricated prototype shows that the main beam can be scanned from 41° to 49° with a gain variation between 13.15 and 15.41 dBi in the frequency range from 56 to 64 GHz. Moreover, confirmation of the design strategy provides the feasibility to realize the system-in-package solution.**

***Index Terms*— Dry etching, folded half-mode waveguide (FHMW), gold plating, leaky-wave antenna (LWA), long slot antenna, silicon bulk micromachining technology, system-in-package (SiP).**

I. Introduction

LEAKY-WAVE antennas (LWAs) exhibit many exciting advantages, such as simple structure, easy to feed, wide bandwidth, high gain, and frequency scanning ability [1]. They can be broadly categorized as the periodic type and continuous type [2]. The periodic type of LWA is generated by introducing periodic perturbations, for example, shorting stubs, dielectric gratings, and slots, to the guiding structure, such as the microstrip line and waveguide [3]–[6]. As a result, a large number of space harmonics are produced, among which the -1 order mode is used most frequently for leaky-wave radiation. Continuous type of LWA means that the guided wave structure is uniform along the propagation direction and fast wave mode is used to couple with the free space for leaky-wave radiation. Waveguide-based long slot is the most common continuous type of LWA and has been studied extensively [7]–[13]. Different shapes and positions of the long slots are selected for various purposes. For example, meander-shaped long slot was adopted to reduce the high sidelobe level that is the drawback of the straight version [11]. Asymmetric ridges were introduced to support the straight long slots located in the centerline of the broad wall to suppress the sidelobe and cross polarization simultaneously [12], [13]. Half-mode substrate integrated waveguide (HMSIW) is another important guided wave structure, whose size is nearly halved compared to the conventional SIW [14], [15]. HMSIW can form leaky-wave radiation from the open side directly by an elaborate design [16], [17], or, more generally, periodic perturbations were loaded to HMSIW, forming the hybrid radiation modes of the periodic and continuous types of LWA [18]–[20]. The inset dielectric waveguide (IDW), which shares the same field distribution with the HMSIW, is also a good candidate for guided wave transmission line [21]. Periodic type of LWA based on IDW was reported by loading metal-strip gratings to the open side [22], and recently, a sinusoidally modulated LWA based on IDW was proposed [23].

Millimeter-wave (MMW) communication around 60 GHz has currently attracted much attention because of the need of higher data rate and better system performance [24]. Consequently, LWAs operating at MMW have been in focus [5], [11], [16], [22], [23], [25], [26]. However, as the MMW LWAs designed using the methods stated above suffer from dielectric loss, antenna efficiency and gain are limited. Long slot LWAs based on all-metallic ridge gap waveguide (RGW) can effectively overcome the dielectric loss problem [25], [26], but because the RGW-based structures

Manuscript received October 14, 2016; revised February 26, 2017; accepted April 15, 2017. Date of publication May 2, 2017; date of current version July 1, 2017. This work was supported in part by the National Basic Research Program of China under Contract 2013CB329002 and in part by the National Natural Science Foundation of China under Contract 61525104. *(Corresponding author: Zhijun Zhang.)*

L. Chang, Z. Zhang, Y. Li, and Z. Feng are with the State Key Lab on Microwave and Communications, Tsinghua National Laboratory for Information Science and Technology, Tsinghua University, Beijing 100084, China (e-mail: zjzh@tsinghua.edu.cn).

S. Wang is with the Hebei Semiconductor Research Institute, Shijiazhuang 050000, China.

Color versions of one or more of the figures in this paper are available online at http://ieeexplore.ieee.org.

Digital Object Identifier 10.1109/TAP.2017.2700040

are nearly 3-D, it is difficult to achieve integration. One of the important merits of the MMW operation is that the small footprint of the MMW devices facilitates antenna-in-package (AiP) solution, which further promotes the system-in-package (SiP) architecture [27]. The SiP technology requires the integration of the antennas and integrated circuits (ICs) on a single package. Thus, the new trend of the MMW antenna design is steering away from the traditional discrete design to AiP configuration [28], [29]. The low-temperature co-fired ceramic (LTCC), which is the mainstream multilayer substrates packaging integrated technology, can fulfill the AiP solution, but the antennas also suffer from dielectric loss and the process is very expensive [30], [31].

Silicon substrate, as one of the most important materials for IC industry, can be used to fabricate MMW antennas for a highly integrated purpose [32]. However, its high permittivity prohibits the silicon-based antennas to achieve high performance. Silicon micromachining is the fundamental technology for fabricating MEMS components, among which, the bulk micromachining, which refers to manipulating the bulk of silicon wafers, can selectively remove the wafer portions for performance-enhancement purpose [33], [34]. Thus, the silicon builds a bridge connecting the antennas and ICs, allowing them to be integrated into a single package, and leading to SiP solution. However, the performance is still limited because the wafer is not entirely removed but is "selectively" removed.

Chang *et al.* [35] have fabricated a purely air-filled antenna using the silicon substrate for the first time based on the silicon bulk micromachining technology. In this paper, an MMW air-filled long slot LWA based on FHMW was fabricated using the same process. Owing to the through-wafer dry etching and gold-plating processes, a purely air-filled L-shaped FHMW is built within three silicon layers without any silicon dielectric being exposed to the air medium. Good leaky-wave performance is realized by the vertical part of the FHMW that can be viewed as the leaky-wave long slot. A matching section and a coupling slot are combined for good impedance matching, and the 410 series waveguide-to-coax transition is used to feed the proposed antenna [35]. Finally, the three silicon layers, an additional copper plate, and the standard WR-15 waveguide-to-coax transition are aligned and clamped together using location pins and screws. Folded HMSIW has been presented for 3-dB coupler design previously [36]. To the best of the authors' knowledge, this is the first time that an FHMW is adopted for antenna design. Compared with the conventional half-mode waveguide, the profile is lowered, the required silicon layer number is fixed to three, and the design can be more flexible. The fabricated prototype shows a measured -10 dB impedance bandwidth of 15.76% from 54.53 to 63.86 GHz and measured scanning beams from 41° to 49° with a gain variation between 13.15 and 15.41 dBi in the frequency range from 56 to 64 GHz. Validity of the design strategy provides the possibility to realize the SiP solutions.

II. L-Shaped Air-Filled Folded Half-Mode Waveguide

Conventional air-filled half-mode waveguide (CAHW), as shown in Fig. 1(a), can be used for leaky-wave radiation directly if it is properly excited and its transverse width is within the single mode operation region, that is, approximately ranging between quarter wavelength at the lowest frequency and half wavelength at the highest frequency, resulting in a rather high profile. Here, the fabrication process is to manipulate the silicon substrate using through-wafer dry etching and gold-plating processes deriving from the silicon bulk micromachining technology, and the mainstream standard thickness of the silicon substrate is 400 μm. The deep groove is generated by stacking multiple silicon layers and each layer has a thin penetration groove inside. At 60 GHz, the groove should be deeper than 1.25 mm regardless of the edge effect; if 400-μm-thick silicon layer is used, four layers are needed in addition to one more layer acting as the shorted ground, as depicted in Fig. 1(b). On the other hand, if customized silicon layer with the required thickness, for example, 1.6 mm is adopted, the dry etching process cannot implement the through-wafer etching. In fact, the through-wafer etching fails as long as the silicon layer is thicker than 1 mm. To reduce the layers and lower the profile, L-shaped air-filled FHMW is proposed as shown in Fig. 1(c), and the practical realization is depicted in Fig. 1(d). Full advantage of the transverse space can be taken by folding the conventional straight half-mode waveguide, and the profile is lowered effectively: a waveguide with any width can be realized by only three layers of silicon.

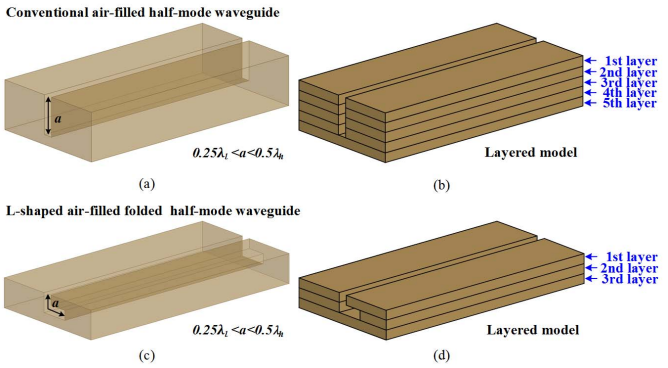

Fig. 1. (a) Geometry of the CAHW. (b) Layered implementation model using 400-μm-thick silicon layers. (λ_l denotes the quarter wavelength at the lowest frequency, and λ_h denotes the half wavelength at the highest frequency.) (c) Geometry of the L-shaped air-filled FHMW. (d) Layered implementation model using 400-μm-thick silicon layers. [All the brown colors with different transparent levels denote the gold, and transparences of the structures in (a)–(d) are set to 0.6, 0, 0.6, and 0, respectively. The blank areas within the silicon layers denote the air medium.]

III. Air-Filled Long Slot Leaky-Wave Antenna Based on Folded Half-Mode Waveguide

A. Antenna Configuration

Configuration of the proposed air-filled long slot LWA is illustrated in Fig. 2(a)–(d), which shows the perspective view, top view, and exploded view of the antenna, and the top view of each layer. The silicon substrate is the 400-μm-thick single-crystal silicon wafer with a permittivity of 11.9 and with total dimensions ($l_t \times w_t$) of 41 × 20 mm^2. The L-shaped air-filled FHMW is composed of two parts: the horizontal part in the middle layer and the vertical part that also acts as the radiating leaky-wave long slot in the top layer. An additional

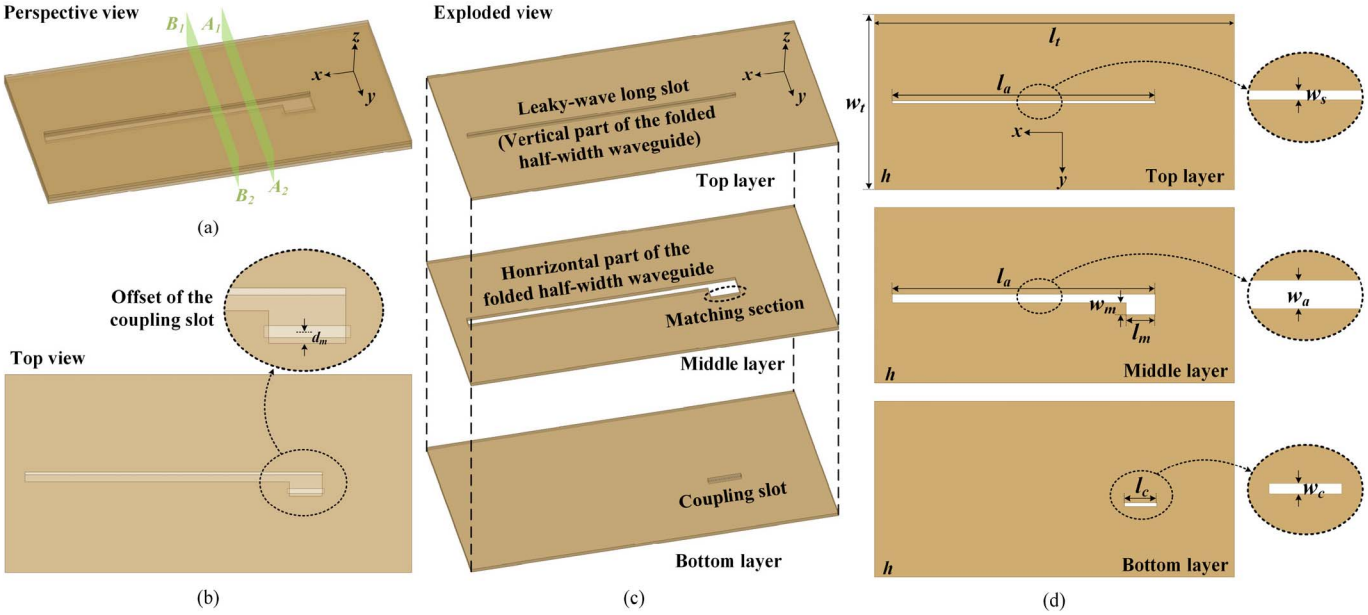

Fig. 2. Configuration of the proposed long slot LWA. (a) Perspective view, (b) top view, (c) exploded view of the antenna, and (d) top view of each layer for dimensions illustration. [All the brown colors with different transparent levels denote the gold, and transparences of the structures in (a)–(d) are set to 0.6, 0.8, 0.6, and 0, respectively. The blank areas within the silicon layers denote the air medium. The proposed antenna is fed by the standard WR-15 waveguide whose center aligns with that of the coupling slot. The uniform L-shaped FHMW section intercepted by A_1A_2 and B_1B_2 planes in (a) is presented in Fig. 3 to depict its dispersion diagram.]

TABLE I
DETAILED DIMENSIONS OF THE PROPOSED ANTENNA (UNIT: mm)

Parameter	l_t	w_t	w_s	l_a	w_a	h
Value	41	20	0.3	30	1	0.4
Parameter	l_m	w_m	l_c	w_c	d_m	
Value	3.35	1.4	3.759	0.5	0.5	

matching section that is integrated with the horizontal part is combined with a coupling slot in the bottom layer for good impedance matching. The length of the long slot (l_a) is 30 mm, and the widths of the horizontal (w_a) and vertical (w_s) parts of the FHMW are 1 and 0.3 mm, respectively. In fact, the total width of the FHMW is 1.4 mm, that is, the sum of the width of horizontal part and the height of the vertical part, and this value lies within the single mode operation region at 60 GHz. The matching section has a length (l_m) of 3.35 mm and a width (w_m) of 1.4 mm. The close-up inset in Fig. 2(b) depicts the offset (d_m) between the coupling slot and matching section; the coupling slot with a length (l_c) of 3.759 mm and a width (w_c) of 0.5 mm aligns with the matching section along y-axis and locates 0.5 mm away from the lower edge of the section. All the dimensions are listed in Table I. In simulation, the proposed antenna is fed using the standard 60-GHz waveguide interface (WR-15) whose center aligns with that of the coupling slot. The numerical results presented in this paper are obtained using the commercial software of High Frequency Structure Simulator (version 14) based on the finite element method.

B. Phase Constant and Attenuation Constant

For an LWA, the phase constant β and attenuation constant α are the two most important parameters that determine the main lobe direction and beamwidth, respectively.

The simulation model of the infinitely long air-filled FHMW is shown in Fig. 3(a). This model aims to obtain the dispersion characteristic by solving an eigenmode problem [37]. The FHMW structure is intercepted by the A_1A_2 and B_1B_2 planes in Fig. 2(a), and the length is set to be infinitely long along the propagation direction (x-axis) using two periodic boundary conditions. The boundary of the top surface is set to perfect magnetic conductor, and the rest of the three surfaces are set to perfect electric conductor (PEC). At the two periodic boundaries, by running a parameter sweep on the variable phase shift ranging from 5° to 180°, the calculated eigenmode frequencies as a function of the phase constant are obtained, as shown in Fig. 3(b). The airline denoted by the dotted line is given for comparison to point out the leaky-wave spectrum: all the frequencies lie in the fast wave area, resulting in leaky-wave radiation. In fact, the leaky radiation region of the proposed antenna is from the cutoff frequency (where the attenuation constant equals the phase constant) to infinitely large. However, due to the bandwidth limitation of the matching network, the actual bandwidth is much narrower.

The normalized attenuation constant is shown in Fig. 4. Here, the attenuation is almost totally caused by radiation without any dielectric loss due to that the proposed antenna is air-filled. As shown, in the frequency band from 55 to 65 GHz, the normalized attenuation constant decreases from 0.096 to 0.057 with the frequency increasing and the variation of the normalized attenuation constant is quite small. If most of the power is radiated, such a small attenuation constant produces long effective aperture, leading to high gain and narrow beamwidth [37]. The design rule of an LWA is to make 90% of the input power radiated, and radiation efficiency η is

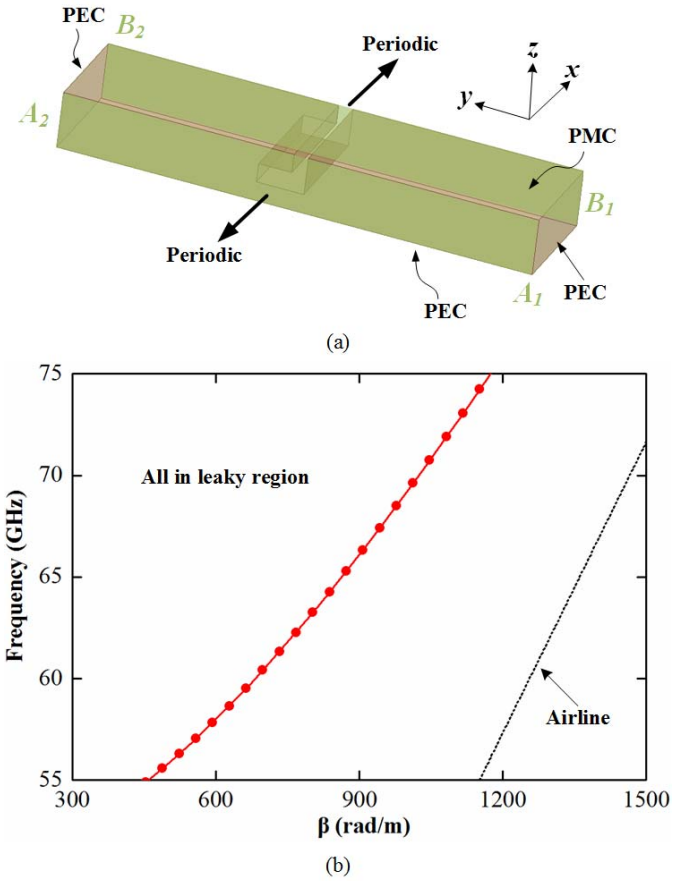

Fig. 3. (a) Simulation model of the infinitely long FHMW used to obtain its dispersion characteristic. (Transparence of the structure is set to 0.6.) (b) Dispersion diagram.

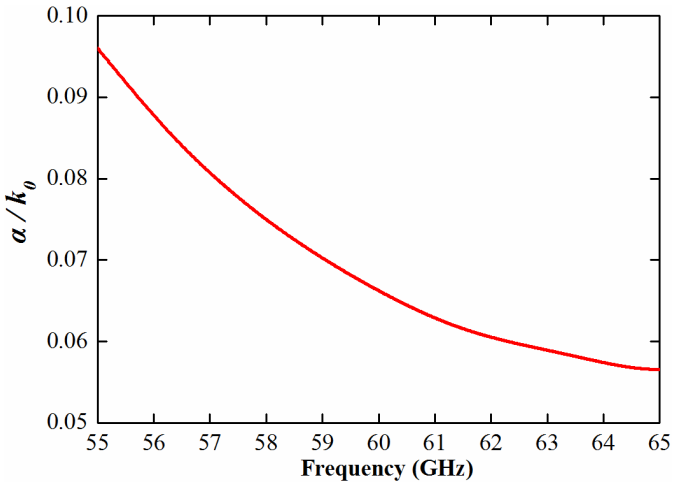

Fig. 4. Normalized attenuation constant of the proposed long slot LWA.

codetermined by the attenuation constant and antenna length

$$\eta = 1 - e^{2\times\alpha\times L} \tag{1}$$

where L is the antenna length. Moreover, there is a certain relationship between attenuation constant and antenna length, and they should be codetermined to make radiation efficiency higher than 90%.

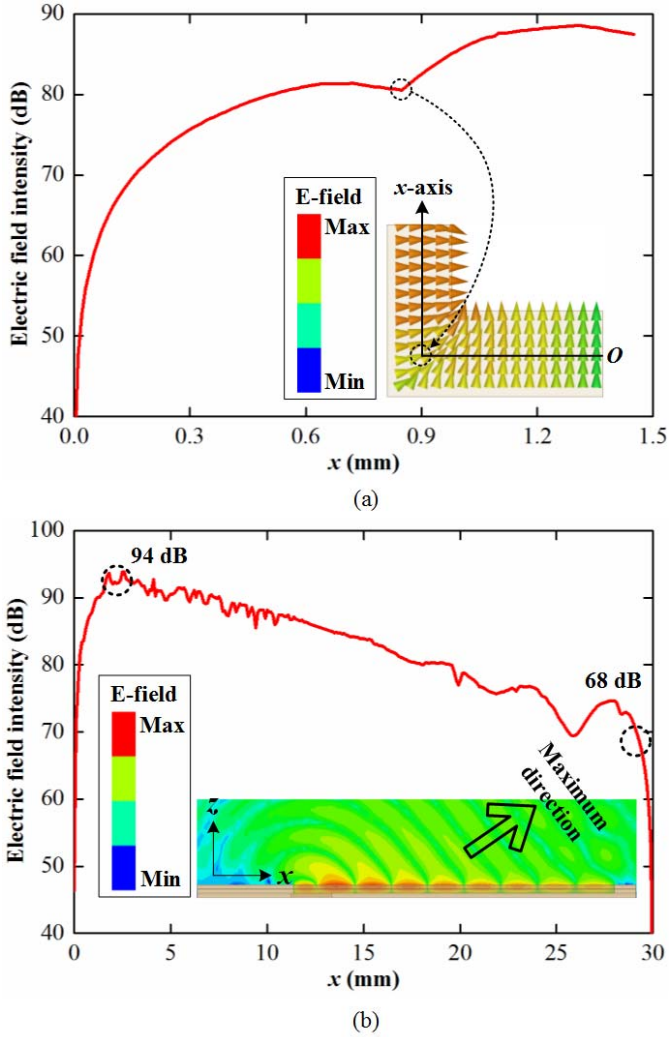

Fig. 5. (a) Vector E-field distribution at the cross section of the FHMW and the E-field intensity along the centerline of the cross section at 60 GHz. (b) Magnitude E-field distribution in the center surface of the long slot and the E-field intensity along the centerline of the long slot at the aperture surface at 60 GHz.

C. Field Distribution

To describe the longitudinal and transverse field distributions, the vector E-field distribution at the cross section of the FHMW and the E-field intensity along the centerline of the cross section at 60 GHz are shown in Fig. 5(a). As seen, the vector E-field distribution is generated by folding half of the TE_{10} mode into "L" shape. The E-field intensity can be approximated by a quarter sinusoid, and the singular point denoted by the dotted circle corresponds to the turning point of the folded waveguide. Thus, it is demonstrated that the field inside the FHMW is similar to the conventional half-mode waveguide [19]. Fig. 5(b) illustrates the magnitude E-field distribution in the center surface of the long slot and the E-field intensity along the centerline of the long slot at the aperture surface at 60 GHz. As seen from the inset, the E-field diminishes gradually and a clear plane wave is observed, indicating the maximum direction as marked. As to the E-field intensity curve, two electric nulls are observed at

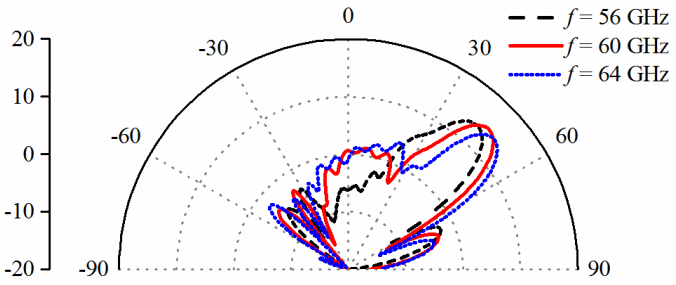

Fig. 6. Frequency scanning beams in H-plane at 56, 60, and 64 GHz.

the starting and ending points, which are caused by the electric wall boundary conditions. The intensity curve in the middle portion approximately depicts the radiating loss: the E-field intensity decreases by 26 dB from the 94 to 68 dB, fulfilling the 90% leaky rate (corresponding to 20-dB intensity decrease) principle [38], and a more lower sampling point selection of the tail end leads to a higher radiation efficiency (exact efficiency will be given in Section V). Thus, from the view of field distribution, the proposed long slot LWA exhibits excellent radiation performance.

IV. Beam Performance

A. Frequency Scanning

The frequency scanning capability of the proposed LWA is depicted in Fig. 6, which shows the H-plane radiation patterns at 56, 60, and 64 GHz. As seen, the main lobe scans from 42° to 48° with an increase in frequency, and the peak gains are all higher than 13.5 dBi. Another merit of the waveguide-based long slot LWA is that the half power beam widths of the scanning beams remain constant, indicating that all the beams are similar in shape. This is different from other common LWAs whose beam widths usually change as the beam scans with frequency [38]. The constant beamwidth performance is explained as follows.

The beamwidth $\Delta\theta$ can be determined by the attenuation constant approximately [39]

$$\Delta\theta \approx \frac{2}{\cos\theta_m} \times \frac{\alpha}{k_0} \tag{2}$$

where θ_m is the maximum direction measured from broadside and k_0 is the wavenumber in free space. The maximum direction is determined by

$$\sin\theta_m = \frac{\beta}{k_0} \tag{3}$$

where β is the phase constant in LWA. For a closed rectangular waveguide with a transverse width of w, the phase constant, cutoff wavenumber k_c, and wavenumber in free space have the following strict relations:

$$\beta^2 + k_c^2 = k_0^2 \tag{4}$$

$$k_c = \frac{\pi}{w} \tag{5}$$

where k_c is a constant with respect to the transverse width. For the proposed open structure, (4) and (5) express the wavenumber relations approximately. Substituting (3)–(5) into (2), the beamwidth can be expressed with only attenuation constant and transverse width

$$\Delta\theta \approx \frac{2 \times \alpha \times w}{\pi}. \tag{6}$$

Thus, the beamwidth is only related to the attenuation constant [39]. As mentioned before, the attenuation constant varies only a little in a 10-GHz bandwidth, so the beamwidth of the proposed antenna remains almost constant.

The constant beamwidth performance is also verified by numerical simulation. The half power beam widths at five frequencies are listed in Table II; as seen, the beam widths are all 13° except for the case of 56 GHz, which is 14°, just a little difference.

TABLE II
Half Power Beam Widths at Different Frequencies

Frequency/GHz	56	58	60	62	64
Beam width	14°	13°	13°	13°	13°

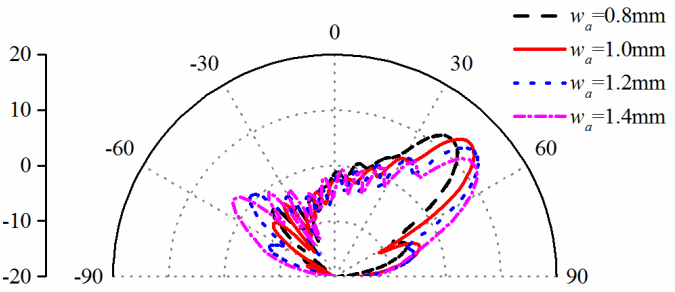

Fig. 7. Directivity patterns at 60 GHz under four different horizontal part widths.

B. Customizing Main Beam Direction

The proposed LWA can customize the beam direction in a certain range at a fixed frequency by selecting the width of the horizontal part of the FHMW without altering the profile. Directivity patterns at 60 GHz under four different widths of the horizontal part are given in Fig. 7. As seen, when the width increases from 0.8 to 1.4 mm, the main beam scans from 40° to 51° and the peak directivities are all higher than 12.3 dBi. The change of the width of the horizontal part causes the change of the cutoff wavenumber of the transverse resonance, that is, the k_c in (4), resulting in the variation of the phase constant β of the LWA; therefore, the main beam direction alters as expressed in (3). Further increasing or decreasing the width makes the proposed FHMW to deviate from the single mode operation or working in the cutoff region, rendering the decrease of the directivity. Thus, the proposed LWA can customize the main beam direction from 40° to 51° at 60 GHz, and the main lobe at other fixed frequencies can be customized as needed as well.

V. Antenna Optimization

Some key parameters that may affect antenna performance are studied. In these parametric studies, only one parameter at a time is adjusted, whereas the others are kept invariant.

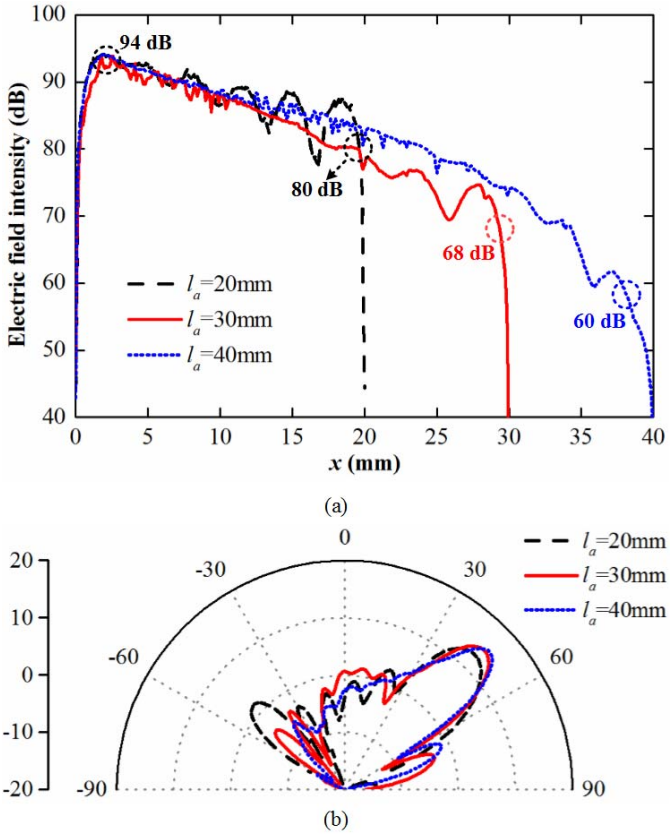

Fig. 8. (a) Electric field intensities along the centerline of the long slot at the aperture surface at 60 GHz. (b) Directivity patterns at 60 GHz under three length cases.

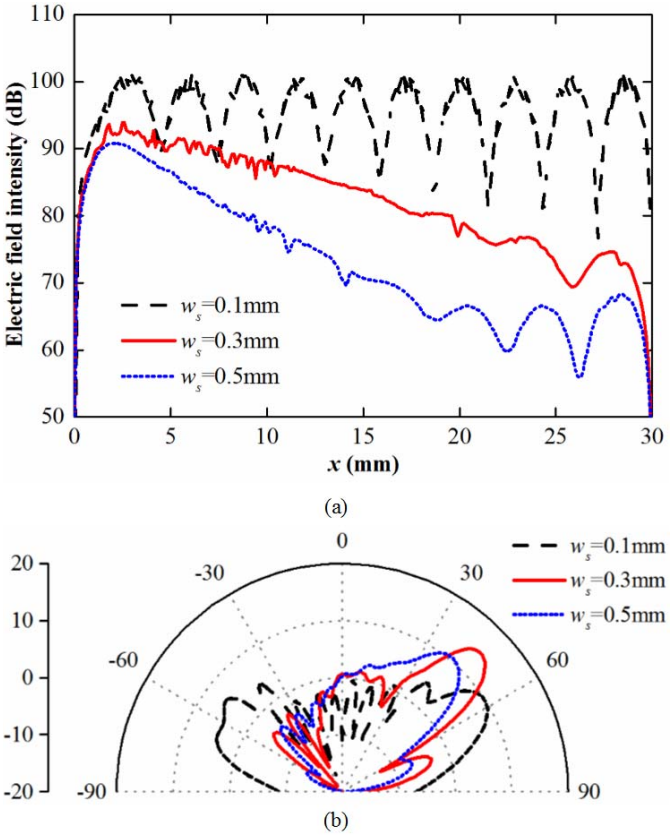

Fig. 9. (a) Electric field intensities along the centerline of the long slot at the aperture surface at 60 GHz. (b) Directivity patterns at 60 GHz under three width cases.

A. Long Slot Length

The length of the long slot is selected according to the principle of more than 90% radiation of the input power, which means that the E-field intensity in the LWA decreases more than 20 dB [38]. The E-field intensities along the centerline of the long slot at the aperture surface under three cases of different slot lengths at 60 GHz are shown in Fig. 8(a). As seen, the E-field intensity decreases from the common maximum value of 94 dB to 80, 68, and 60 dB for the lengths of 20, 30, and 40 mm, respectively. The intensity decrement of the 20-mm case is less than 20 dB, only about 14 dB. The leftover power that is not radiated propagates backward, producing a high sidelobe whose direction is symmetrical with the main lobe, and the peak directivity is relatively small, as verified by the directivity pattern shown in Fig. 8(b). The 30- and 40-mm cases satisfy the "20-dB condition" and have very nearly the same decrement, that is, 26 and 34 dB, respectively. As shown in Fig. 8(b), the patterns of the two cases are similar and their peak directivities are 14.48 and 14.96 dBi; this means that the extra 8-dB decrease of the 40-mm case has weak contribution to radiation. Thus, the length of the proposed LWA is selected as 30 mm. According to (1), this length and the attenuation constant make the proposed antenna radiating more than 99% of the input power without considering impedance matching in the band 55–65 GHz. If the impedance matching is taken in to consideration, in the final realized frequency band (56.44–63.82 GHz), more than 88.62% of the input power is radiated by the proposed LWA.

B. Long Slot Width

Effect of the long slot width on radiation performance is studied in Fig. 9(a) and (b), which shows the E-field intensities along the long slot and the directivity patterns under three cases of different slot widths at 60 GHz. As the slot width is 0.1 mm, the E-field intensity exhibits sinusoidal periodic distribution and the peak magnitude of each period remains constant, indicating that the electromagnetic wave inside the long slot presents the standing wave style. This is caused by the fact that the long slot is too narrow to radiate effectively; therefore the backward wave that possesses almost equal energy superposes the forward wave, producing the standing wave. As shown in Fig. 9(b), peak directivity of the pattern is only 9.9 dBi. As the width is 0.5 mm, the E-field intensity drops rapidly: the 20-dB decrement position locates at about the middle of the long slot, the second half of the long slot contributes little to radiation. The pattern of the 0.5-mm case shows a peak directivity of only 10.48 dBi. The situation of the 0.3-mm case falls in between the former two cases: the long slot is wide enough to leak into free space effectively and the E-field attenuation rate along the aperture remains at a proper level, resulting in a relatively uniform aperture amplitude distribution, producing a beam with good quality.

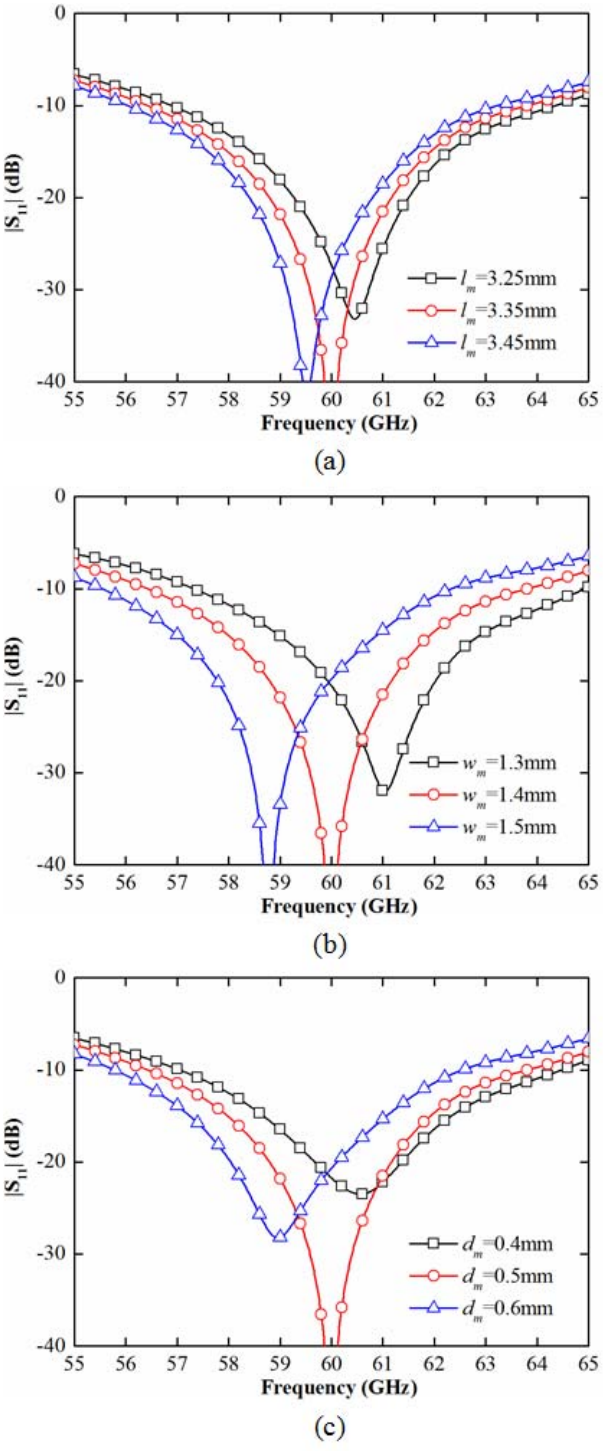

Fig. 10. Simulated $|S_{11}|$ of the proposed antenna under different (a) lengths and (b) widths of the matching section, and (c) offsets between the coupling slot and matching section.

C. Impedance Matching

Dimensions of the matching section have influence on the impedance matching, and the impacts of the length and width variations on the magnitude of reflection coefficient are depicted in Fig. 10(a) and (b). As the dimension increases or decreases by 0.1 mm, the influence of the width variation is more severe than that of the length variation. However, the variation of ±0.1 mm causes only slight change in reflection coefficient, implying that the matching condition is robust to the dimensions of the matching section. The offset of the coupling slot and matching section also has impact on impedance matching, as shown in Fig. 10(c). As seen, the impedance matching is not that sensitive to the change of the offset, but the matching condition is best when the offset is 0.5 mm. Moreover, the micromachining accuracy is far more precise than 0.1 mm. Thus, the matching approach adopted here is so robust, leading to stable antenna performance.

In conclusion, all the critical parameters that are proved to be the optimum solutions make the antenna exert its best performance.

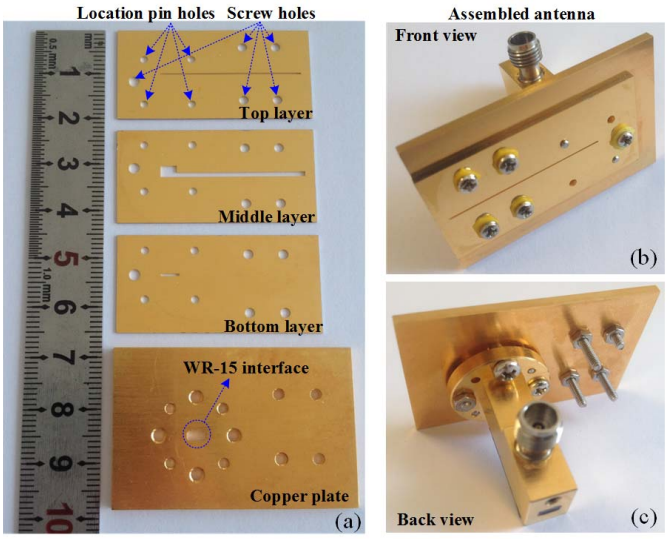

Fig. 11. Photographs of the fabricated long slot LWA. (a) Top views of the silicon substrates and copper plate. (b) Front and (c) Back views of the antenna assembled using the 410 series waveguide-to-coax transition.

VI. Fabrication and Experimental Result

A. Silicon Bulk Micromachining Process

The proposed air-filled long slot LWA is fabricated using silicon bulk micromachining technology. The photographs of the three silicon substrate layers, a 2-mm-thick copper plate, and the whole antenna are depicted in Fig. 11(a)–(c). The 410 series waveguide-to-coax transition is used to connect the assembled antenna (including the three silicon layers and the copper plate) and vector network analyzer (VNA) for measurement purpose. The copper plate with a standard WR-15 waveguide inside has twofold functions: 1) connecting the feeding waveguide and the three silicon layers and 2) protecting the three fragile silicon layers, and clamping them together tightly.

The fabrication technique contains two processes deriving from the silicon bulk micromachining technology, that is, through-wafer dry etching and gold plating, among which the former is the core for designing air-filled antenna using the high-permittivity silicon. In the first step, the penetration structures, including the horizontal part of the FHMW,

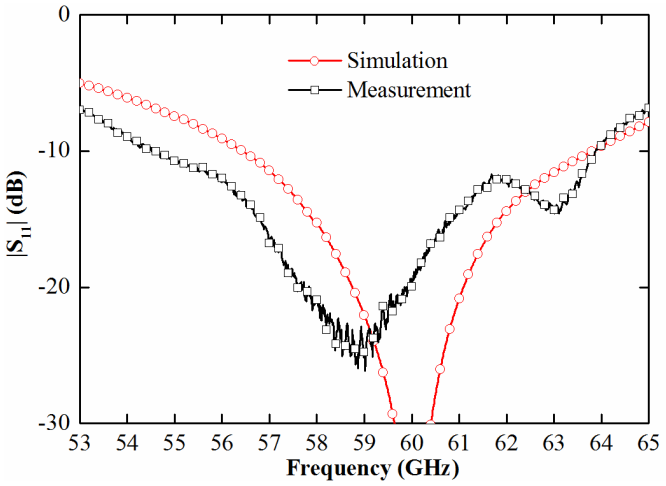

Fig. 12. Simulated and measured $|S_{11}|$ of the proposed long slot LWA.

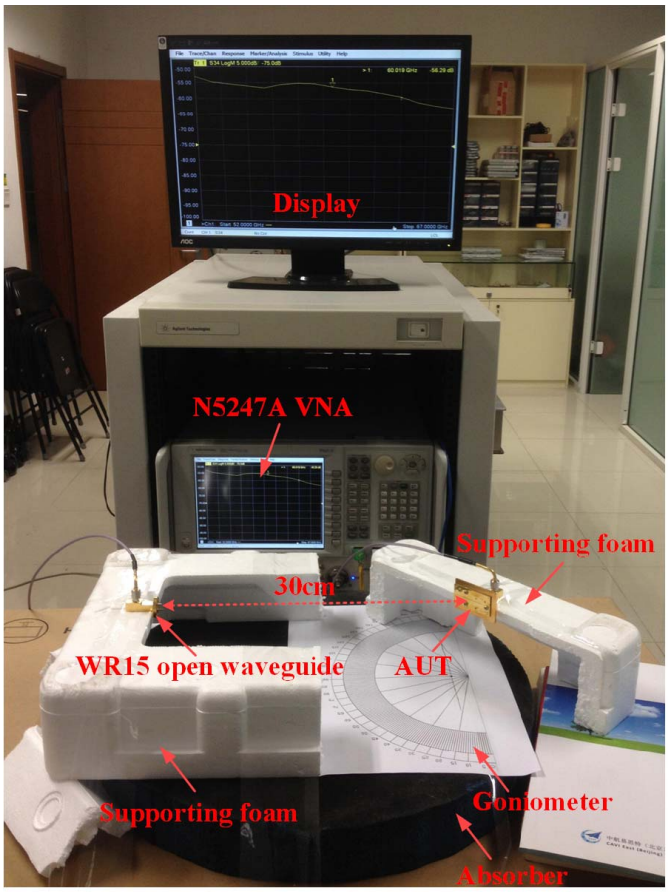

Fig. 13. Measurement setup.

the vertical part of the FHMW and the matching section, the coupling slots, and all the location holes, are all etched away using dry etching process with sulfur hexafluoride gas. The etching ensures a high precision of about ± 4 μm. Then, all the faces and sidewalls of the three silicon layers are plated with a 3.5-μm-thick gold layer with the tolerance of ± 0.5 μm. At this stage, no silicon dielectric is exposed outside and the electromagnetic wave interacts only with air medium, forming

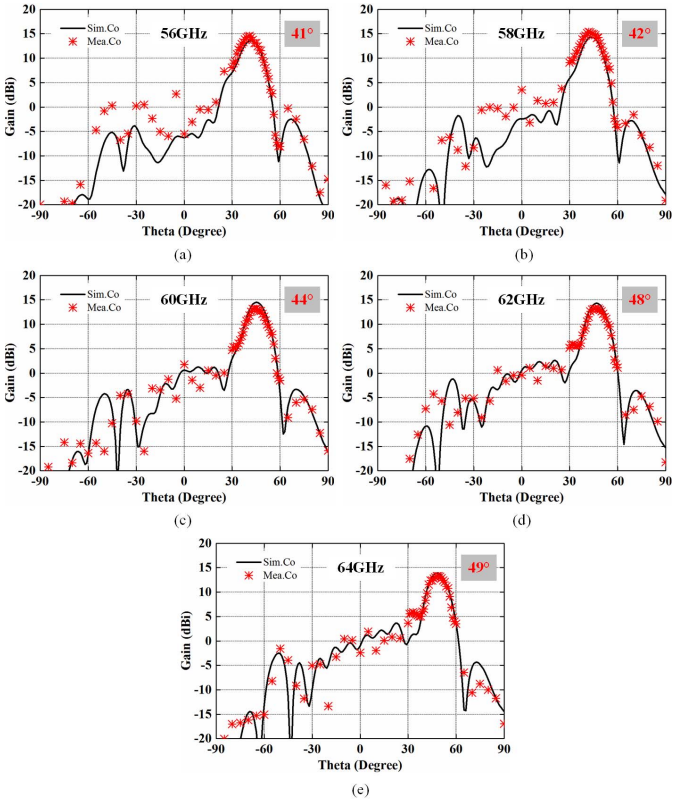

Fig. 14. Simulated and measured H-plane patterns at 56, 58, 60, 62, and 64 GHz of the proposed long slot LWA. (The maximum directions are marked in each pattern.)

TABLE III
SIMULATED AND MEASURED MAXIMUM DIRECTIONS, PEAK GAINS, AND HALF POWER BEAM WIDTHS OF THE PROPOSED ANTENNA

Frequency/GHz		56	58	60	62	64
Maximum direction	Sim.	42°	44°	45°	47°	48°
	Mea.	41°	42°	44°	48°	49°
Peak gain/dBi	Sim.	13.56	14.30	14.48	14.29	13.93
	Mea.	14.57	15.41	13.15	13.19	13.29
Beam width	Sim.	14°	13°	13°	13°	13°
	Mea.	14°	14°	13°	12°	13°

a purely air-filled antenna. Finally, the three silicon layers, the copper plate, and the waveguide-to-coax transition are aligned and clamped together with location pins and screws.

B. Impedance Bandwidth and Radiation Patterns

The reflection coefficient and radiation patterns were measured using a N5247A VNA (10 MHz–67 GHz). The simulated and measured magnitudes of reflection coefficient are shown in Fig. 12. The simulated bandwidth is 12.27% from 56.44 to 63.82 GHz, whereas the measured bandwidth is 15.76% from 54.53 to 63.86 GHz for $|S_{11}| < -10$ dB. They agree well with each other, and the small discrepancy mainly comes from the fabrication error.

The measurement setup for achieving the radiation patterns is shown in Fig. 13. The standard WR-15 open waveguide, that is, the 410 series waveguide-to-coax transition acted as the

receiving antenna and gain calibration antenna simultaneously. The distance between the antenna under test (AUT) (AUT, proposed antenna) and receiving antenna was 30 cm, and the AUT was rotated manually with the help of a printed goniometer and only the forward radiation was measured. A piece of wave absorber was placed underneath to create a stable test environment. Within the angle range from $+30°$ to $+60°$ containing the main lobes, the sampling interval angle is 1°; out of this region, the sampling interval angle is 5°. Fig. 14 shows the simulated and measured H-plane patterns at 56, 58, 60, 62, and 64 GHz. As seen, the measured patterns agree well with the simulation. The maximum directions, peak gains, and half power beam widths are listed in Table III. Experiment of the fabricated prototype shows that the main beam can be scanned from 41° to 49° with a gain variation between 13.15 and 15.41 dBi, and the half power beamwidth varies between 12° and 14° in the frequency range from 56 to 64 GHz. The maximal errors of the maximum direction, peak gain, and beamwidth are 2°, 1.4 dB, and 1°, respectively, between the measurement and simulation. The errors mainly comes because of manual testing; as illustrated in Fig. 13, when measuring the pattern and gain, the AUT was rotated by 1° in each sampling step around the maximum direction, and this procedure together with the alignment between the AUT and receiving antenna was accomplished fully by sight with the help of the printed goniometer. It is difficult to obtain an accurate result just by visual inspection, even though, the measured result is still acceptable. Therefore, the fabrication accuracy is so high that the silicon bulk micromachining technology is very suitable for manufacturing MMW, or even terahertz antenna.

As stated in [35], if the input interface is changed from the waveguide-to-coax transition to waveguide-to-ground-signal-ground transition, the proposed long slot LWA can be integrated with ICs within a single package, promoting the SiP solution.

VII. Conclusion

This paper combines the novel folded half-mode waveguide (FHMW) and silicon bulk micromachining technology to realize an air-filled long slot LWA using silicon substrate. Through-wafer dry etching and gold-plating processes are adopted to manipulate the silicon substrate, generating a purely air-filled antenna within three silicon layers without any silicon dielectric being exposed to the air medium. To the best of the authors' knowledge, this is the first time that an FHMW is adopted for antenna design. Compared with the conventional half-mode waveguide, the profile is lowered, the required silicon layer number is fixed to three, and the design can be more flexible. Measurement of the antenna prototype shows good performance. Thanks to this fabrication process, antenna engineers can boldly design antennas using silicon substrate that is one of the most important materials for ICs, allowing the integration of antennas and ICs, thus promoting SiP solutions. We have confirmed this point and the SiP product is already available.

References

[1] J. Sheen and Y.-D. Lin, "Propagation characteristics of the slotline first higher order mode," *IEEE Trans. Microw. Theory Techn.*, vol. 46, no. 11, pp. 1774–1781, Nov. 1998.

[2] D. R. Jackson, C. Caloz, and T. Itoh, "Leaky-wave antennas," *Proc. IEEE*, vol. 100, no. 7, pp. 2194–2206, Jul. 2012.

[3] Y. Li, Q. Xue, E. K. N. Yung, and Y. Long, "The periodic half-width microstrip leaky-wave antenna with a backward to forward scanning capability," *IEEE Trans. Antennas Propag.*, vol. 58, no. 3, pp. 963–966, Mar. 2010.

[4] Y. Li, Q. Xue, H.-Z. Tan, and Y. Long, "The half-width microstrip leaky wave antenna with the periodic short circuits," *IEEE Trans. Antennas Propag.*, vol. 59, no. 9, pp. 3421–3423, Sep. 2011.

[5] F. K. Schwering and S.-T. Peng, "Design of dielectric grating antennas for millimeter-wave applications," *IEEE Trans. Microw. Theory Tech.*, vol. 31, no. 2, pp. 199–209, Feb. 1983.

[6] J. Liu, D. R. Jackson, and Y. Long, "Substrate integrated waveguide (SIW) leaky-wave antenna with transverse slots," *IEEE Trans. Antennas Propag.*, vol. 60, no. 1, pp. 20–29, Jan. 2012.

[7] L. Goldstone and A. Oliner, "Leaky-wave antennas I: Rectangular waveguides," *IEEE Trans. Antennas Propag.*, vol. 7, no. 4, pp. 307–319, Oct. 1959.

[8] P. Bonnaval, "Directional slot antenna for very high frequencies," U.S. Patent 3 978 485 A, Aug. 31, 1976.

[9] G. S. Scharp, "Continuous slot antennas," U.S. Patent 4 328 502 A, May 4, 1982.

[10] L. Goldstone and A. Oliner, "Leaky wave antennas II: Circular waveguides," *IEEE Trans. Antennas Propag.*, vol. 9, no. 3, pp. 280–290, May 1961.

[11] Y. J. Cheng, W. Hong, K. Wu, and Y. Fan, "Millimeter-wave substrate integrated waveguide long slot leaky-wave antennas and two-dimensional multibeam applications," *IEEE Trans. Antennas Propag.*, vol. 59, no. 1, pp. 40–47, Jan. 2011.

[12] A. Mallahzadeh and S. Mohammad-Ali-Nezhad, "Long slot ridged SIW leaky wave antenna design using transverse equivalent technique," *IEEE Trans. Antennas Propag.*, vol. 62, no. 11, pp. 5445–5452, Nov. 2014.

[13] S. Mohammad-Ali-Nezhad and A. Mallahzadeh, "Periodic ridged leaky-wave antenna design based on SIW technology," *IEEE Antennas Wireless Propag. Lett.*, vol. 14, pp. 354–357, Feb. 2015.

[14] B. Liu, W. Hong, Y.-Q. Wang, Q.-H. Lai, and K. Wu, "Half mode substrate integrated waveguide (HMSIW) 3-dB coupler," *IEEE Microw. Wireless Compon. Lett.*, vol. 17, no. 1, pp. 22–24, Jan. 2007.

[15] Q. Lai, C. Fumeaux, W. Hong, and R. Vahldieck, "Characterization of the propagation properties of the half-mode substrate integrated waveguide," *IEEE Trans. Microw. Theory Techn.*, vol. 57, no. 8, pp. 1996–2004, Aug. 2009.

[16] J. Xu, W. Hong, H. Tang, Z. Kuai, and K. Wu, "Half-mode substrate integrated waveguide (HMSIW) leaky-wave antenna for millimeter-wave applications," *IEEE Antennas Wireless Propag. Lett.*, vol. 7, pp. 85–88, 2008.

[17] N. Nguyen-Trong, T. Kaufmann, and C. Fumeaux, "A wideband omnidirectional horizontally polarized traveling-wave antenna based on half-mode substrate integrated waveguide," *IEEE Antennas Wireless Propag. Lett.*, vol. 12, pp. 682–685, 2013.

[18] A. Pourghorban Saghati, M. M. Mirsalehi, and M. H. Neshati, "A HMSIW circularly polarized leaky-wave antenna with backward, broadside, and forward radiation," *IEEE Antennas Wireless Propag. Lett.*, vol. 13, pp. 451–454, 2014.

[19] Q. H. Lai, W. Hong, Z. Q. Kuai, Y. S. Zhang, and K. Wu, "Half-mode substrate integrated waveguide transverse slot array antennas," *IEEE Trans. Antennas Propag.*, vol. 57, no. 4, pp. 1064–1072, Apr. 2009.

[20] D. K. Karmokar, K. P. Esselle, and S. G. Hay, "Fixed-frequency beam steering of microstrip leaky-wave antennas using binary switches," *IEEE Trans. Antennas Propag.*, vol. 64, no. 6, pp. 2146–2154, Jun. 2016.

[21] M. Guglielmi and G. Boccalone, "A novel theory for dielectric-inset waveguide leaky-wave antennas," *IEEE Trans. Antennas Propag.*, vol. 39, no. 4, pp. 497–504, Apr. 1991.

[22] M. Guglielmi and D. R. Jackson, "Broadside radiation from periodic leaky-wave antennas," *IEEE Trans. Antennas Propag.*, vol. 41, no. 1, pp. 31–37, Jan. 1993.

[23] X. Bai, S.-W. Qu, K.-B. Ng, and C. H. Chan, "Sinusoidally modulated leaky-wave antenna for millimeter-wave application," *IEEE Trans. Antennas Propag.*, vol. 64, no. 3, pp. 849–855, Mar. 2016.

[24] P. Smulders, "Exploiting the 60 GHz band for local wireless multimedia access: Prospects and future directions," *IEEE Commun. Mag.*, vol. 40, no. 1, pp. 140–147, Jan. 2002.
[25] M. Al Sharkawy and A. Kishk, "Long slots array antenna based on ridge gap waveguide technology," *IEEE Trans. Antennas Propag.*, vol. 62, no. 10, pp. 5399–5403, Oct. 2014.
[26] M. Al Sharkawy, A. Foroozesh, A. A. Kishk, and R. Paknys, "A robust horn ridge gap waveguide launcher for metal strip grating leaky wave antenna," *IEEE Trans. Antennas Propag.*, vol. 62, no. 12, pp. 6019–6029, Dec. 2014.
[27] Y. P. Zhang and D. Xian, "Antenna-on-chip and antenna-in-package solutions to highly integrated millimeter-wave devices for wireless communications," *IEEE Trans. Antennas Propag.*, vol. 57, no. 10, pp. 2830–2841, Oct. 2009.
[28] T. M. Shen, T. Y. J. Kao, T. Y. Huang, J. Tu, J. Lin, and R. B. Wu, "Antenna design of 60-GHz micro-radar system-in-package for noncontact vital sign detection," *IEEE Antennas Wireless Propag. Lett.*, vol. 11, pp. 1702–1705, 2012.
[29] A. Mahanfar, S.-W. Lee, A. M. Parameswaran, and R. G. Vaughan, "Self-assembled monopole antennas with arbitrary shapes and tilt angles for system-on-chip and system-in-package applications," *IEEE Trans. Antennas Propag.*, vol. 58, no. 9, pp. 3020–3028, Sep. 2010.
[30] S.-H. Wi *et al.*, "Package-level integrated antennas based on LTCC technology," *IEEE Trans. Antennas Propag.*, vol. 54, no. 8, pp. 2190–2197, Aug. 2006.
[31] J.-H. Lee *et al.*, "Highly integrated millimeter-wave passive components using 3-D LTCC system-on-package (SOP) technology," *IEEE Trans. Antennas Propag.*, vol. 53, no. 6, pp. 2220–2229, Jun. 2005.
[32] K. K. O *et al.*, "On-chip antennas in silicon ICs and their application," *IEEE Trans. Electron Devices*, vol. 52, no. 7, pp. 1312–1323, Jul. 2005.
[33] I. Papapolymerou, R. F. Drayton, and L. P. B. Katehi, "Micromachined patch antennas," *IEEE Trans. Antennas Propag.*, vol. 46, no. 2, pp. 275–283, Feb. 1998.
[34] J.-G. Yook and L. P. B. Katehi, "Micromachined microstrip patch antenna with controlled mutual coupling and surface waves," *IEEE Trans. Antennas Propag.*, vol. 49, no. 9, pp. 1282–1289, Sep. 2001.
[35] L. Chang, Z. Zhang, Y. Li, S. Wang, and Z. Feng, "60-GHz air substrate leaky-wave antenna based on MEMS micromachining technology," *IEEE Trans. Compon., Packag. Manuf. Technol.*, vol. 6, no. 11, pp. 1656–1662, Nov. 2016.
[36] G. H. Zhai *et al.*, "Folded half mode substrate integrated waveguide 3 dB coupler," *IEEE Microw. Wireless Compon. Lett.*, vol. 18, no. 8, pp. 512–514, Aug. 2008.
[37] D. K. Karmokar, K. P. Esselle, and T. S. Bird, "Wideband microstrip leaky-wave antennas with two symmetrical side beams for simultaneous dual-beam scanning," *IEEE Trans. Antennas Propag.*, vol. 64, no. 4, pp. 1262–1269, Apr. 2016.
[38] A. A. Oliner and D. R. Jackson, "Leaky-wave antennas," in *Antenna Engineering Handbook*, J. L. Volakis, Ed. New York, NY, USA: McGraw-Hill, 2007, ch. 11.
[39] D. R. Jackson and A. A. Oliner, "Leaky-wave antennas," in *Modern Antenna Handbook*, C. A. Balanis, Ed. Hoboken, NJ, USA: Wiley, 2008, ch. 7.

Le Chang (S'16) received the B.S. degree in electronics and information engineering from Xidian University, Xi'an, China, in 2012. He is currently pursuing the Ph.D. degree in electrical engineering with Tsinghua University, Beijing, China.

His current research interests include antenna design and theory, particularly in antenna arrays based on transmission lines, transmitted arrays, leaky-wave antennas, and millimeter-wave and terahertz antennas based on silicon micromachining technology.

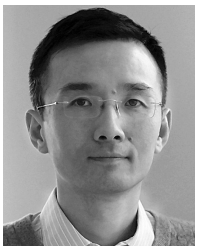

Zhijun Zhang (M'00–SM'04–F'15) received the B.S. and M.S. degrees from the University of Electronic Science and Technology of China, Chengdu, China, in 1992 and 1995, respectively, and the Ph.D. degree from Tsinghua University, Beijing, China, in 1999.

In 1999, he was a Post-Doctoral Fellow with the Department of Electrical Engineering, University of Utah, Salt Lake City, UT, USA, where he was appointed as a Research Assistant Professor in 2001. In 2002, he was an Assistant Researcher with the University of Hawaii at Manoa, Honolulu, HI, USA. In 2002, he joined Amphenol T&M Antennas, Vernon Hills, IL, USA, as a Senior Staff Antenna Development Engineer and was then promoted to the position of Antenna Engineer Manager. In 2004, he joined Nokia Inc., San Diego, CA, USA, as a Senior Antenna Design Engineer. In 2006, he joined Apple Inc., Cupertino, CA, USA, as a Senior Antenna Design Engineer and was then promoted to the position of Principal Antenna Engineer. Since 2007, he has been with Tsinghua University, where he is a Professor with the Department of Electronic Engineering. He has authored Antenna Design for Mobile Devices (Wiley, 2011).

Dr. Zhang served as the Associate Editor of the IEEE TRANSACTIONS ON ANTENNAS AND PROPAGATION during 2010–2014 and the IEEE ANTENNAS AND WIRELESS PROPAGATION LETTERS during 2009–2015.

Yue Li (S'11–M'12) received the B.S. degree in telecommunication engineering from the Zhejiang University, Zhejiang, China, in 2007, and the Ph.D. degree in electronic engineering from Tsinghua University, Beijing, China, in 2012.

In 2012, he was a Post-Doctoral Fellow in the Department of Electronic Engineering, Tsinghua University. In 2013, he was a Research Scholar in the Department of Electrical and Systems Engineering, University of Pennsylvania Philadelphia, PA, USA. He was also a Visiting Scholar in Institute for Infocomm Research, A*STAR, Singapore, in 2010, and Hawaii Center of Advanced Communication, University of Hawaii at Manoa, Honolulu, HI, USA, in 2012. Since 2016, he has been with Tsinghua University, where he is an Assistant Professor with the Department of Electronic Engineering. He has authored or co-authored for 80 journal papers and over 30 international conference papers, and holds 15 granted Chinese patents. His current research interests include metamaterials, plasmonics, nanocircuits, electromagnetics, mobile and handset antennas, MIMO and diversity antennas, and millimeter-wave antennas and arrays.

Shaodong Wang photograph and biography are not available at the time of publication.

Zhenghe Feng (M'05–SM'08–F'12) received the B.S. degree in radio and electronics from Tsinghua University, Beijing, China, in 1970.

Since 1970, he has been with Tsinghua University, as an Assistant, Lecture, Associate Professor, and Full Professor. His current research interests include numerical techniques and computational electromagnetics, RF and microwave circuits and antenna, wireless communications, smart antenna, and spatial temporal signal processing.